## Supporting Information

# Metal Array Fabrication based on Ultrasound-Induced Self-Assembly of Metalated Dipeptides

Katsuhiro Isozaki,[a,b,c] Yusuke Haga,[a] Kazuki Ogata,[b] Takeshi Naota[a], and Hikaru Takaya,[a,b,d*]

[a]Department of Chemistry, Osaka University, 1-3 Machikaneyama, Toyonaka, Osaka 560-8531, Japan, [b]Institute for Chemical Research, Kyoto University, Gokasyo, Uji, Kyoto 611-0011, Japan, [c]National Institute for Materials Science, 1-1 Namiki, Tsukuba, Ibaraki 311-0044, Japan, [d]PRESTO, Japan Science and Technology Agency.

**Variable concentration $^1$H NMR experiments of $\mathbf{1}_{\mathbf{PdPd}}$ in $CDCl_3$.** $^1$H NMR spectra of $\mathbf{1}_{\mathbf{PdPd}}$ in $CDCl_3$ were measured at several concentration (0.195, 0.390, 0.781, 1.56, 3.13, 12.5, 50.0, and 100 mM) at 293 K (Figure S1). As a result, it is revealed that imine protons and amide protons were downfield shifted along with increasing the concentration. These concentaration dependent downfield shifts suggests the existence of intramolecular hydrogen bonds between palladium moiety and amides through chlorine atoms.

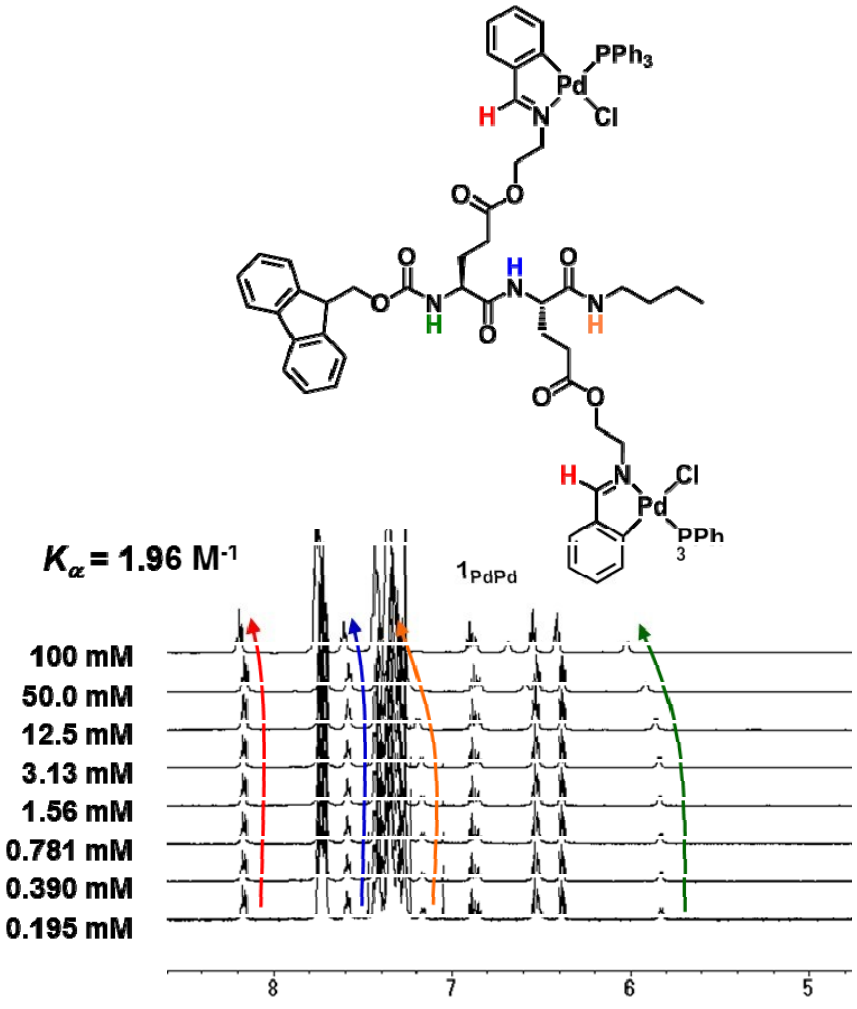


**Figure S1.** Variable concentration (0.195 – 100 mM) $^1$H NMR spectra of $\mathbf{1}_{\mathbf{PdPd}}$ in $CDCl_3$

**Variable temperature $^1$H NMR experiments of $\mathbf{1}_{PdPd}$ in EtOAc-*d8*.** $^1$H NMR spectra of **1a** (3.00 mM) in EtOAc-*d8* were measured at several temperature (298, 303, 308, 313, 318, 323, 328, 333, 338, and 343 K) (Figure S2). This result revealed that imine protons and amide protons were upfield shifted with elevating temperature. These temperature dependent upfield shifts supports the existence of intramolecular hydrogen bonds between palladium moiety and amides through chlorine atoms.

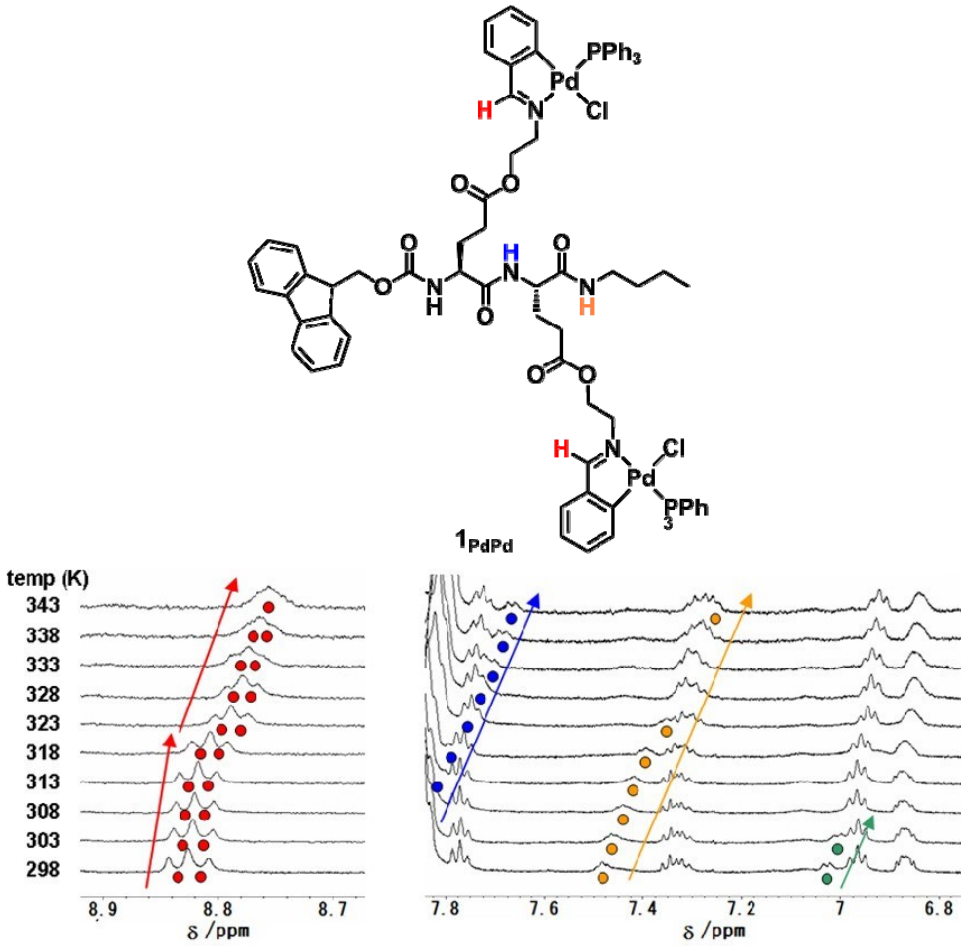


**Figure S2.** Imine and amide regions of $^1$H NMR spectra of **1a** in EtOAc-*d8*.

**Association experiments for analysing the equilibrium constant (*K*a) between PdCl- 5a and PtCl-benzaldimine complexes 5b with *N*-methylacetamide.** $^1$H NMR spectra were measured for $CDCl_3$ solution containing *N*-methylacetamide (NMA: $4.00 \times 10^{-3}$ M) and several contents ($1.60$, $0.80$, $0.40$, and $0.20 \times 10^{-4}$ M) of **5a** or **5b**. Downfield shifts of amide proton of NMA were observed with increasing of complex contents (Figure S3 and S4). This downfield shift shows the adduct formation between complex **5a** or **5b** and NMA based on hydrogen bonds. The equilibrium constants were calculated using Benesi-Hildebrand equation 1,[2] where, $K_a$ is the equilibrium constant, $A_f$ is the chemical shift of free host, $A_{ob}$ is the observed chemical shift in the presence of various guest contents, and $A_{fc}$ is the

$$\frac{1}{(A_f - A_{ob})} = \frac{1}{(A_f - A_{fc})} + \frac{1}{K_a(A_f - A_{fc})[\text{guest}]} \qquad (1)$$

chemical shift at saturation. The relationship between $1/(A_f-A_{ob})$ and 1/[guest] was shown in Figure S3. The linear dependence of $1/(A_f-A_{ob})$ on the reciprocal of the guest concentration indicates the formation of a 1:1 molecular complex between complex **5a** or **5b** and NMA.

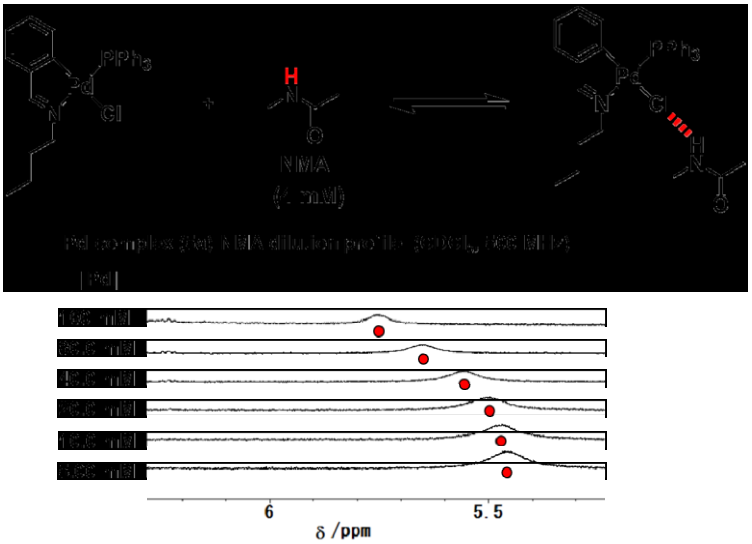


**Figure S3.** Variable concentration $^1$H NMR experiment for Benesi-Hildebrand plots on the association of **5a** and NMA in $CDCl_3$.

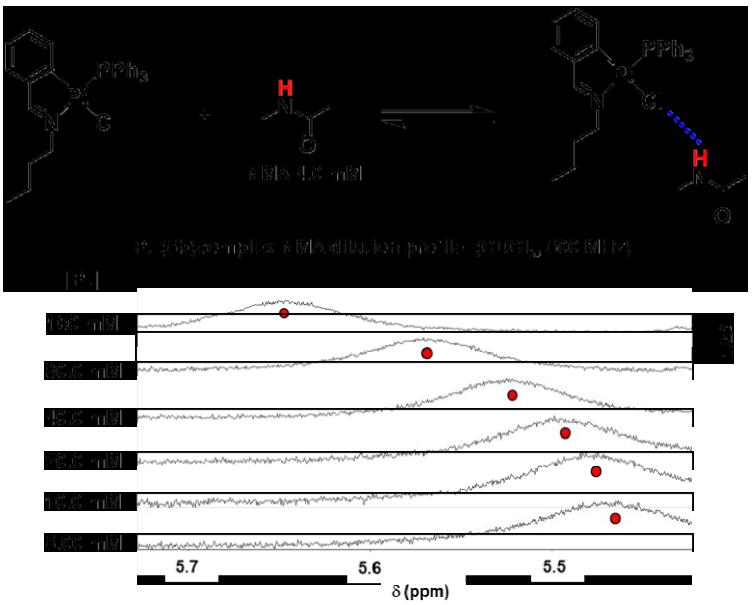


**Figure S4.** Variable concentration $^1$H NMR experiment for Benesi-Hildebrand plots on the association of **5b** and NMA in $CDCl_3$.

**Comparison of $^1$H NMR downfield shifts of α-imino hydrogen of Pd-complexes in $CDCl_3$.** $^1$H NMR spectra of *O*-acetyl-protected **6a**, **6a**, and $\mathbf{1}_{\mathbf{PdPd}}$ (3.00 mM) in $CDCl_3$ were measured at 298K (Figure S5). The observed downfield shifts of **5a** and $\mathbf{1}_{\mathbf{PdPd}}$ strongly suggested Pd–Cl•••H–N intramolecular hydrogen bond.

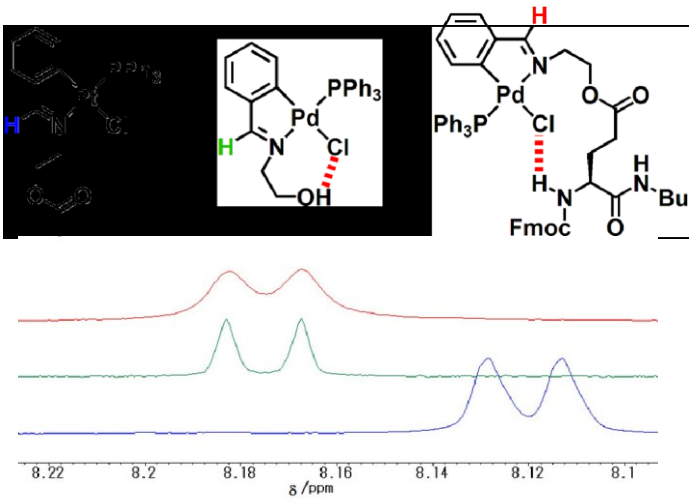


**Figure S5.** $^{1}$H NMR spectra of *O*-acetyl-protected **5a**, **5a**, and $\mathbf{1_{PdPd}}$ in $CDCl_3$.

**Computational methods.** The NBO charges of the complex **6a** and **6b** were obtained from DFT calculations using crystal structures of them. The optimization was carried out using the Gaussian03[1] programs implementation of DFT (B3LYP) with LanL2DZ basis.

**Variable concentration UV-vis experiments of $\mathbf{1_{PdPd}}$ in $CDCl_3$.** UV-vis spectra of $\mathbf{1_{PdPd}}$ in $CDCl_3$ were measured at several concentration (0.195, 0.391, 0.781, 1.56, 3.13, 6.25, 12.5, 25, 50, and 100 mM) at 293 K (Figure S6). Hypochromicity was observed at the range of 215 – 281 nm under the high concentration conditions. In the AcOEt gel, there was no absorbance in the region from 215 to 256 nm related to the Fmoc moiety of $\mathbf{1_{PdPd}}$.

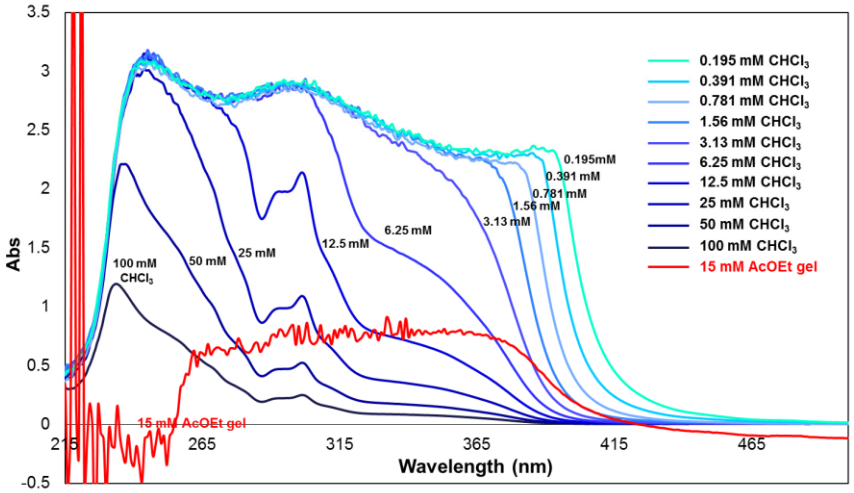


**Figure S6.** Variable concentration UV-vis spectra of $\mathbf{1_{PdPd}}$ in $CDCl_3$ and UV-vis spectrum of AcOEt gel state (red line).

**References**

1) Frisch, M. J.; Trucks, G. W.; Schlegel, H. B.; Scuseria, G. E.; Robb, M. A.; Cheeseman, J. R.; Montgomery, Jr. J. A.; Vreven, T.; Kudin, K. N.; Burant, J. C.; Millam, J. M.; Iyengar, S. S.; Tomasi, J.; Barone, V.; Mennucci, B.; Cossi, M.; Scalmani, G.; Rega, N.; Petersson, G. A.; Nakatsuji, H.; Hada, M.; Ehara, M.; Toyota, K.; Fukuda, R.; Hasegawa, J.; Ishida, M.; Nakajima, T.; Honda, Y.; Kitao, O.; Nakai, H.; Klene, M.; Li, X.; Knox, J. E.; Hratchian, H. P.; Cross, J. B.; Adamo, C.; Jaramillo, J.; Gomperts, R.; Stratmann, R. E.; Yazyev, O.; Austin, A. J.; Cammi, R.; Pomelli, C.; Ochterski, J. W.; Ayala, P. Y.; Morokuma, K.; Voth, G. A.; Salvador, P.; Dannenberg, J. J.; Zakrzewski, V. G.; Dapprich, S.; Daniels, A. D.; Strain, M. C.; Farkas, O.; Malick, D. K.; Rabuck, A. D.; Raghavachari, K.; Foresman, J. B.; Ortiz, J. V.; Cui, Q.; Baboul, A. G.; Clifford, S.; Cioslowski, J.; Stefanov, B. B.; Liu, G.; Liashenko, A.; Piskorz, P.; Komaromi, I.; Martin, R. L.; Fox, D. J.; Keith, T.; Al-Laham, M. A.; Peng, C. Y.; Nanayakkara, A.; Challacombe, M.; Gill, P. M. W.; Johnson, B.; Chen, W.; Wong, M. W.; Gonzalez, C.; Pople, J. A. Gaussian, Inc., Pittsburgh, PA, 2003.

2) Neelakandan, P. P.; Hariharan, M.; Ramaiah, D. *Org. Lett.* **2005**, *7*, 5765.

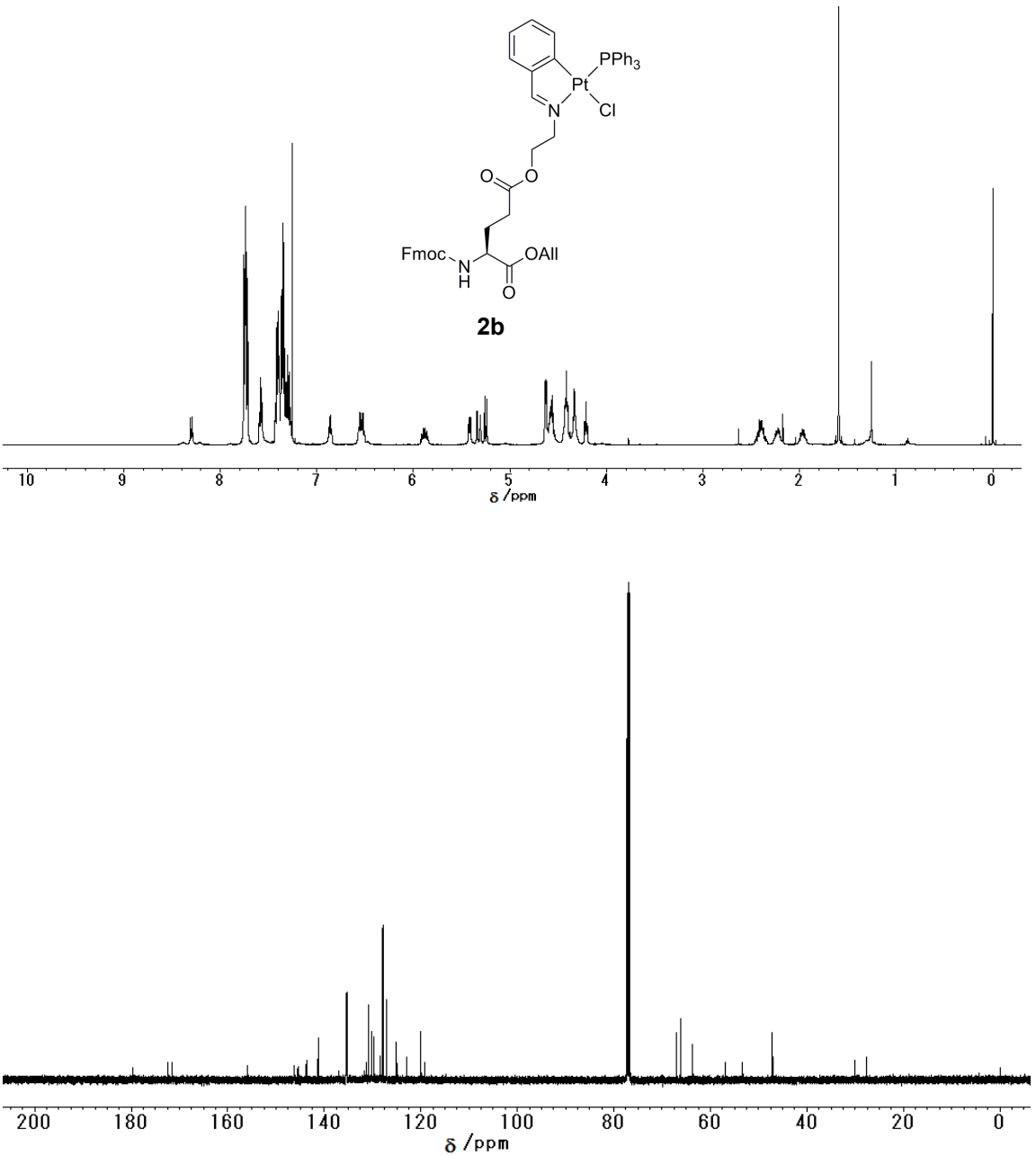


**Figure S7.** $^{1}H$ and $^{13}C$ NMR spectra of **2b**.

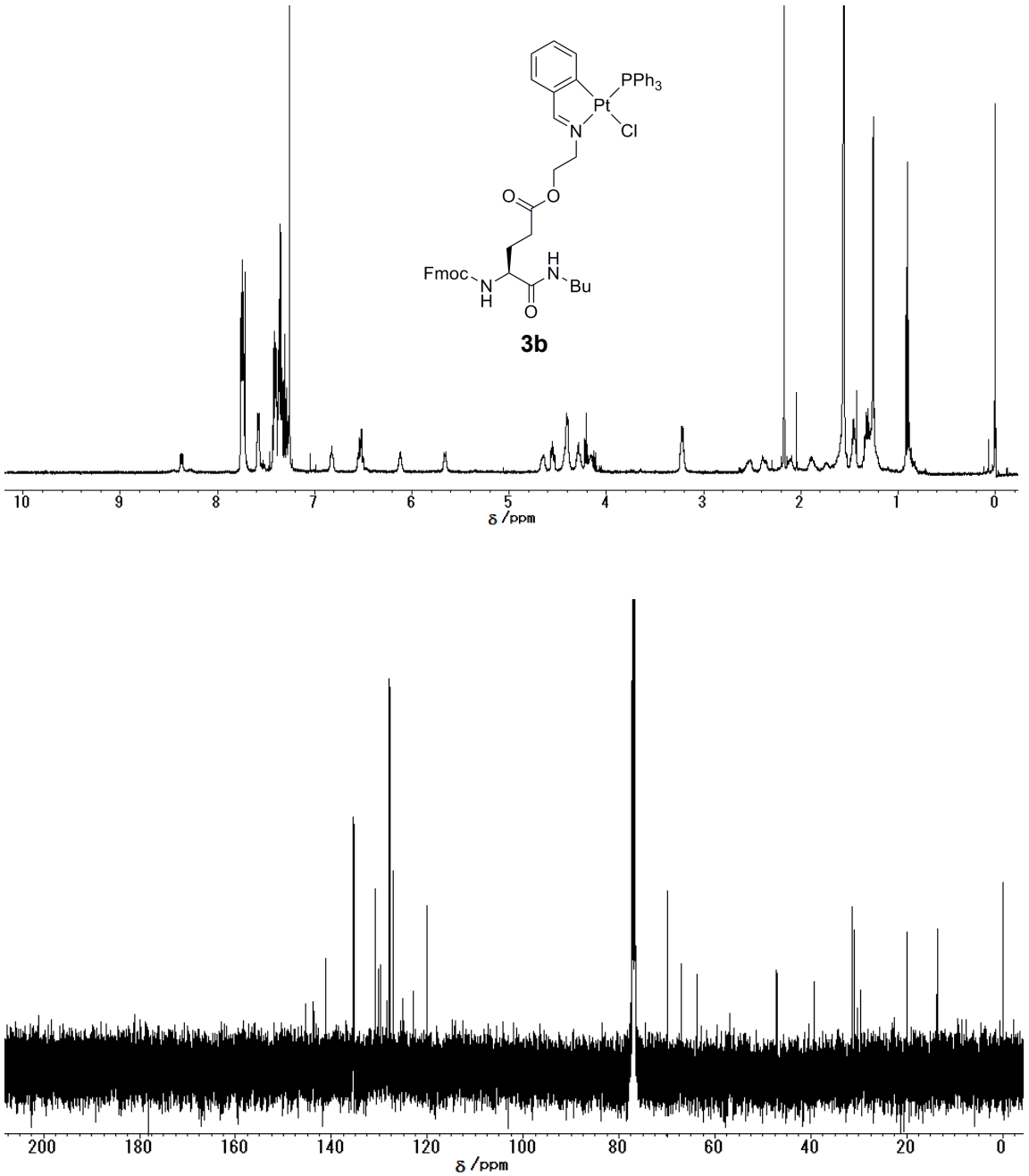


**Figure S8.** $^{1}H$ and $^{13}C$ NMR spectra of **3b**.

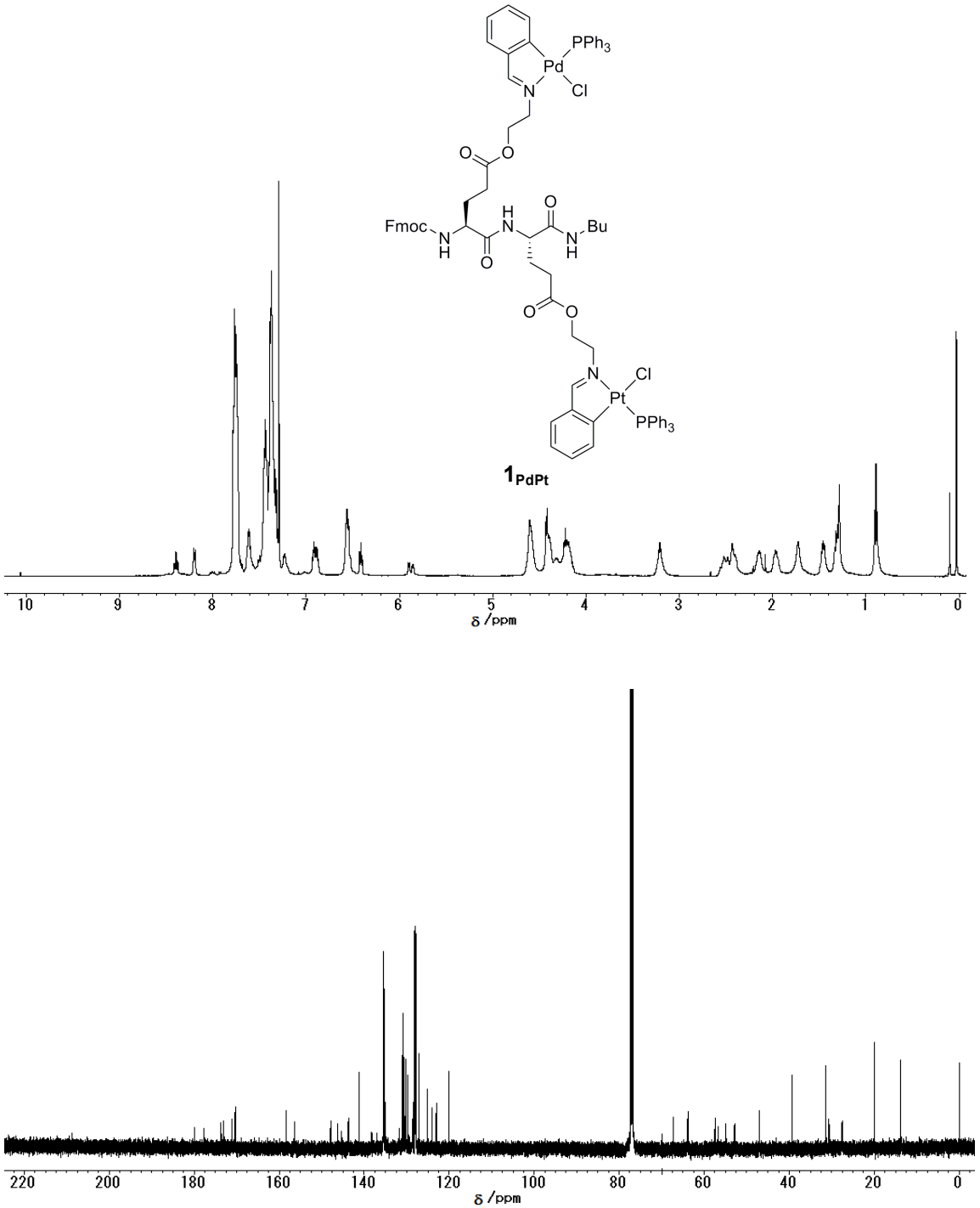


**Figure S9.** $^{1}H$ and $^{13}C$ NMR spectra of $\mathbf{1}_{\mathbf{PdPt}}$.

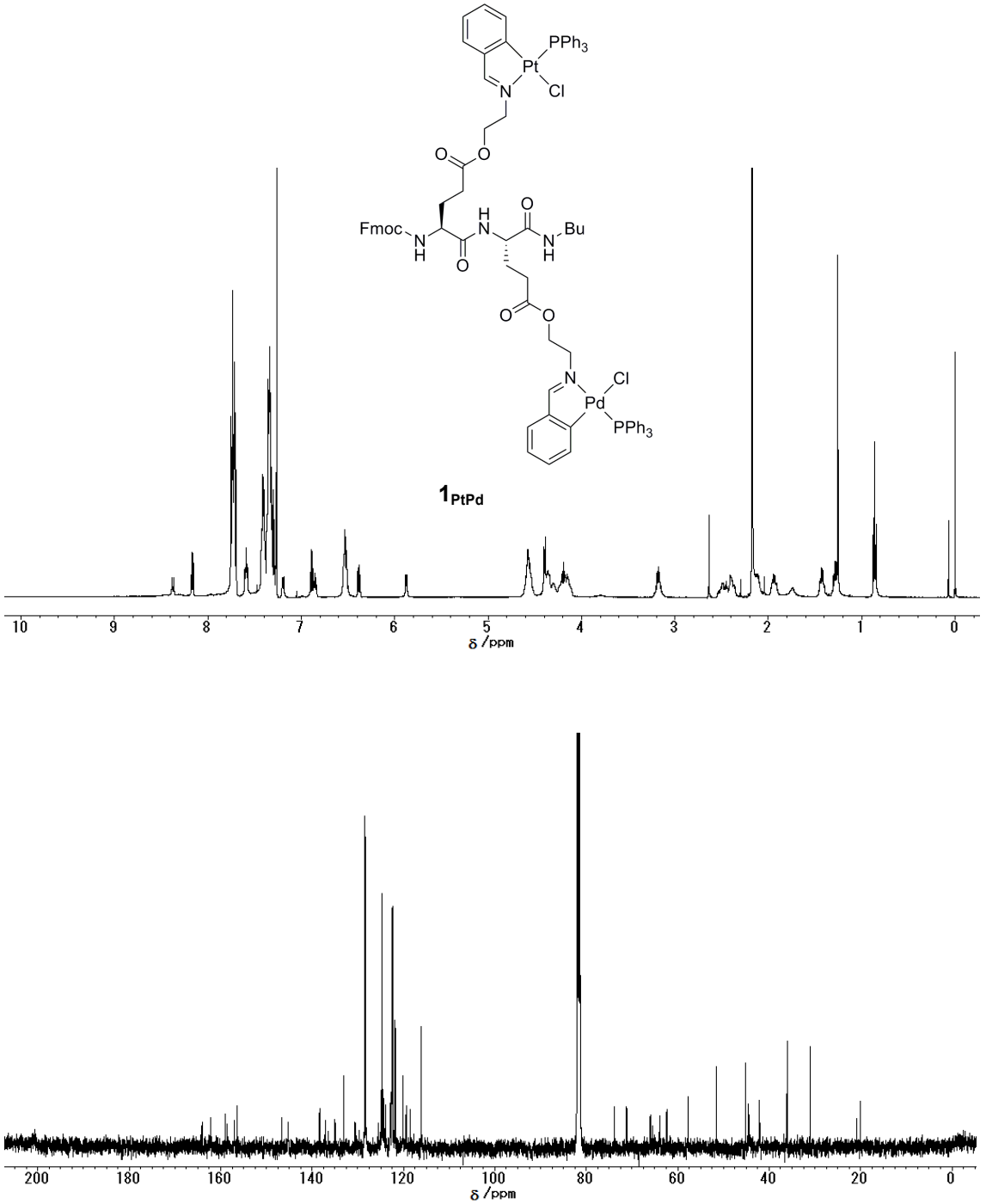


**Figure S10.** $^{1}H$ and $^{13}C$ NMR spectra of $\mathbf{1_{PtPd}}$.

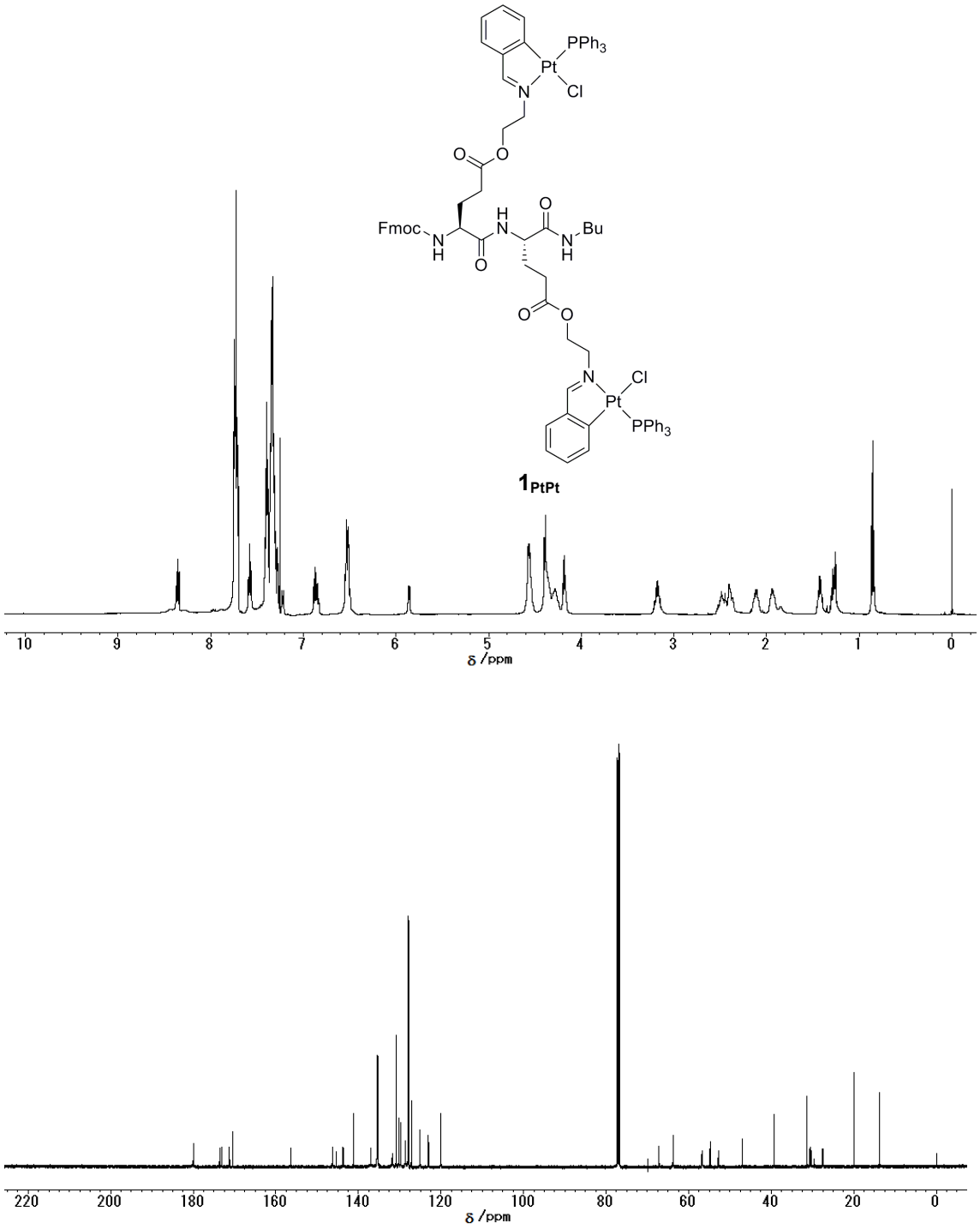


**Figure S11.** $^{1}H$ and $^{13}C$ NMR spectra of $\mathbf{1_{PtPt}}$.

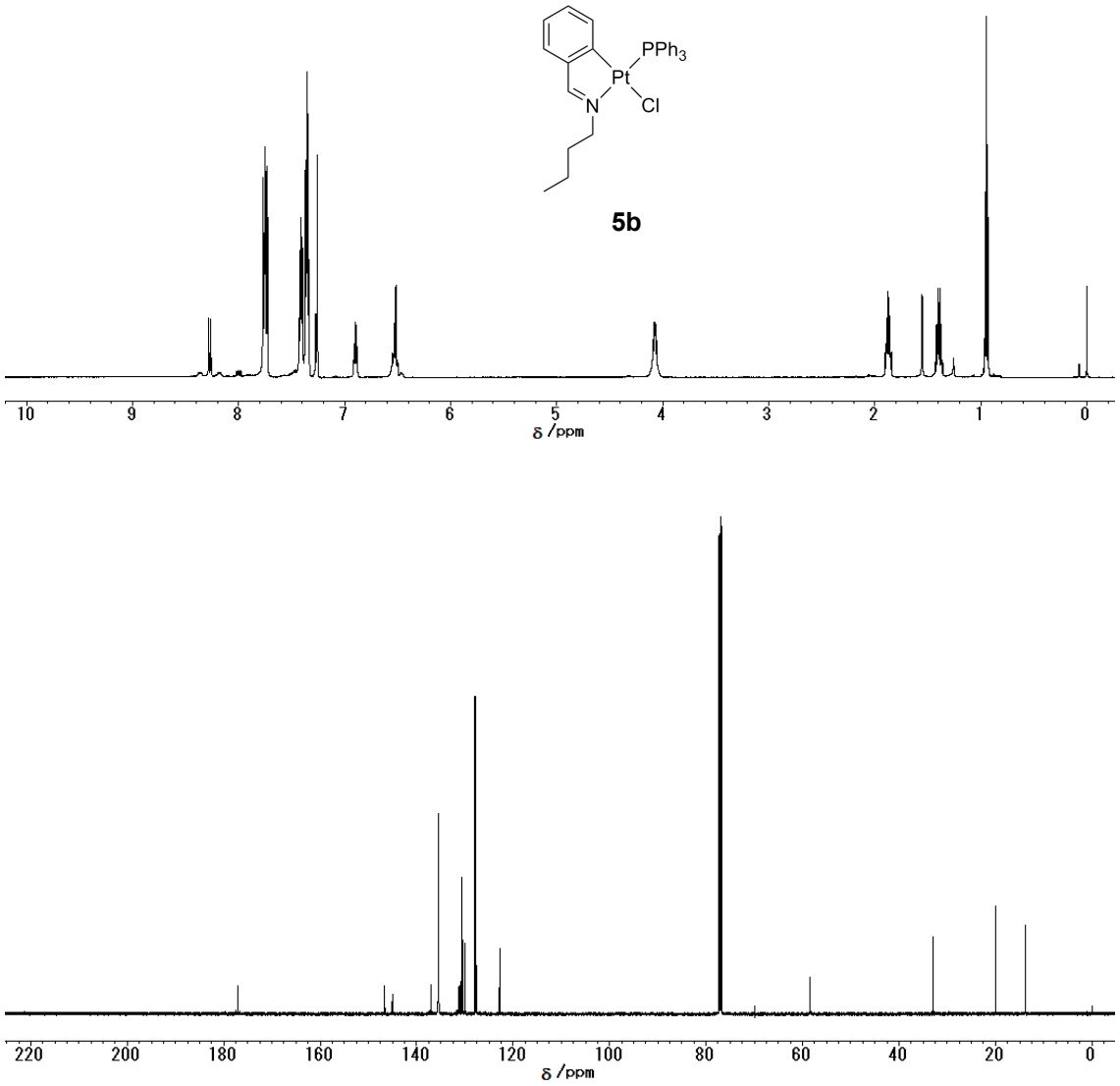


**Figure S12.** $^{1}H$ and $^{13}C$ NMR spectra of **5b**.